JOURNAL OF CATALYSIS **131,** 491–501 (1991)

# An *in Situ* EXAFS Investigation of Bimetallic Cu-Ni/$\gamma$-$Al_2O_3$ Catalysts[1]

G. U. KULKARNI, G. SANKAR, AND C. N. R. RAO[2]

*Solid State and Structural Chemistry Unit, Indian Institute of Science, Bangalore 560012, India*

Received November 9, 1990; revised April 26, 1991

*In situ* EXAFS investigations have been carried out on Ni/$\gamma$-$Al_2O_3$ and Cu-Ni/$\gamma$–$Al_2O_3$ catalysts with different metal loadings, and prepared by different procedures. As-prepared Ni/$\gamma$-$Al_2O_3$ on calcination gives NiO and $NiAl_2O_4$-like phases on the surface, the proportion of the latter increasing with the increase in calcination temperature; the proportion of the NiO-like phase, on the other hand, increases with the metal loading. The reducibility of Ni/$\gamma$-$Al_2O_3$ to give metallic Ni on the surface directly depends on the proportion of the NiO-like phase present before reduction. Co-impregnating with Cu suppresses the formation of the surface aluminate and thereby favours the reduction to metallic Ni. This conclusion is clearly substantiated by our studies of bimetallic catalysts containing varying Cu/Ni ratios and also those prepared by the two-stage impregnation procedure.

## INTRODUCTION

The catalytic performance of bimetallic catalysts is known to differ significantly from that of the individual components, often showing mutual promotion effects towards reduction (*1–3*) and increasing the thermal stability against sintering. Alloying of nickel with copper, for example, modifies the activity of the former in the hydrogenation of ethylene (*4*), benzene (*5*), and butadiene (*6*). Addition of Rh or Ru metal promoters significantly improves the stability of Ni/$Al_2O_3$ catalyst toward sintering (*7*). There have been several characterization studies on monometallic Cu/$\gamma$-$Al_2O_3$ and Ni/$\gamma$-$Al_2O_3$ catalysts. On the basis of optical, magnetic (*8*), ESR, EXAFS (*9*), and X-ray photoelectron spectroscopic (*10*) and temperature programmed reduction (*11*) measurements, it has been suggested that at low loading levels, the metal ions form surface aluminates ($NiAl_2O_4$, $CuAl_2O_4$). With an increase in metal loading, the monoxides (NiO, CuO) segregate out. It appears that the extent of reducibility depends on the reducibility behaviour of the aluminates. Characterization of silica-supported Ni–Cu catalysts has been reported by Bernardo *et al.* (*12*) who also review the early literature on this bimetallic system.

An earlier *ex situ* EXAFS study (*13*) on Cu–Ni/$\gamma$-$Al_2O_3$ catalysts has indicated the presence of $Ni^{2+}$, $Ni^0$, $Cu^{1+}$, and $Cu^0$ in the reduced catalysts, the relative proportions of the different species depending on the composition. In this paper, we report results of a detailed investigation of the bimetallic Cu–Ni/$\gamma$-$Al_2O_3$ catalyst system in both the calcined and reduced states by *in situ* EXAFS measurements. The power of EXAFS in unravelling certain detailed features of such complex catalyst systems has been well documented (*14*). In order to understand the interaction of Ni with $\gamma$-$Al_2O_3$, we have carried out measurements on the Ni/$\gamma$-$Al_2O_3$ system as a function of the calcination temperature as well as the metal loading. We have prepared the bimetallic Cu–Ni/$\gamma$-$Al_2O_3$ catalysts by different procedures in order to clearly understand the competing behaviour of nickel and copper in forming aluminates with the $\gamma$-$Al_2O_3$ support and also to understand the mutual promo-

---

[1] Contribution No. 726 from Solid State and Structural Chemistry Unit.

[2] To whom correspondence should be addressed.

0021-9517/91 $3.00

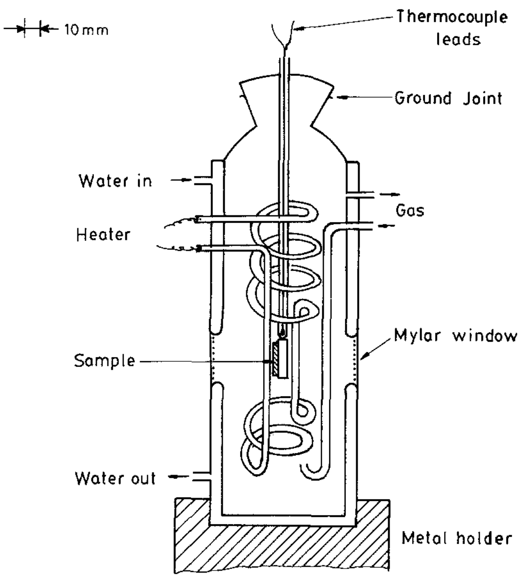

FIG. 1. Schematic diagram of the *in-situ* EXAFS cell made of quartz.

tion effects of Ni and Cu towards reduction. The study has indeed established that copper promotes the reduction of nickel, whereas copper itself is easily reducible.

## EXPERIMENTAL

### *Catalyst Preparation*

The catalyst samples were prepared by the pore-volume impregnation of $\gamma$-$Al_2O_3$ (200 $m^2/g$) with aqueous solutions of $Ni(NO_3)_2$ and $Cu(NO_3)_2$ in appropriate ratios. We have prepared four types of catalysts as discussed below.

1. 5 wt.% of Ni on $\gamma$-$Al_2O_3$, calcined at different temperatures (370, 570, 770, and 970 K) for 3h (4 samples).
2. Bimetallic Cu–Ni/$\gamma$-$Al_2O_3$ catalysts with a total metal loading of 5 wt.% with Ni to Cu ratios of 75 : 25, 50 : 50 and 25 : 75 along with samples containing the same loading of Cu and Ni alone (5 samples).
3. Bimetallic Cu–Ni/$\gamma$-$Al_2O_3$ catalysts with a fixed Ni concentration (2.5 wt.%) but varying Ni to Cu ratios of 75 : 25, 50 : 50, and 25 : 75 along with samples containing Ni and Cu (each 2.5 wt.%) alone (5 samples).
4. Two samples with a Ni to Cu ratio of 50 : 50 (each 2.5 wt.%) prepared by two-stage impregnation. In this method, the support was impregnated by one metal after another with an intermediate calcination at 770 K for 3 h.

The catalyst samples of categories 2, 3, and 4 were calcined at 770 K for 3 h after drying at 370 K for 12 h. Reductions were carried out in an all-quartz *in situ* EXAFS cell at 770 K for 3 h.

### *Apparatus and Procedure*

The *in situ* EXAFS cell consists of a double-walled quartz tube having a ground joint at the top and closed at the bottom (Fig. 1). The sample heating element enclosed in a spiral quartz tube passes from the sides of the cell along with the gas inlet–outlet tubes. The sample in the form of a pellet of 20 mm diameter is mounted on a quartz sample holder hanging from the ground joint at the top. The sample holder contains a thermocouple just below the sample, to monitor the temperature. The cell has Mylar windows for transmission of X-rays and water was circulated through the double-walled cell in order to cool the ground joint and the Mylar windows.

The EXAFS spectra were recorded at room temperature using an X-ray absorption spectrometer (Rigaku, Japan) with a ro-

TABLE 1

Structural Parameters of Reference Systems

| System | Atom pair | Interatomic distance $R$(Å) | Coordination number $N$ |
|---|---|---|---|
| Cu metal | Cu–Cu | 2.56 | 12 |
| $Cu_2O$ | Cu–O | 1.84 | 2 |
| | Cu–Cu | 3.02 | 12 |
| $CuAl_2O_4$ | Cu–O | 1.91 | 4 |
| | Cu–O | 1.93 | 6 |
| Ni metal | Ni–Ni | 2.48 | 12 |
| NiO | Ni–O | 2.08 | 6 |
| $NiAl_2O_4$ | Ni–O | 1.83 | 4 |
| | Ni–O | 1.97 | 6 |

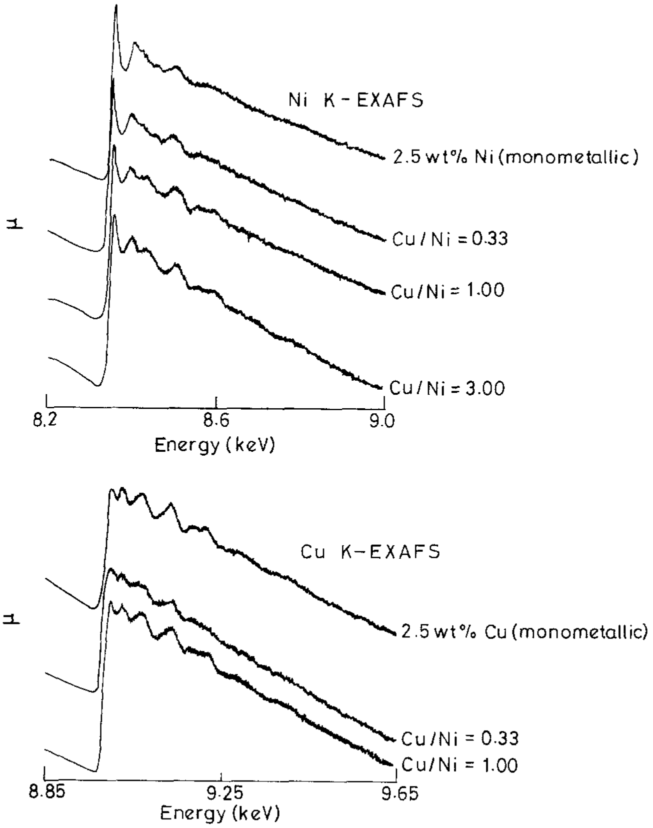

FIG. 2. Raw EXAFS data of reduced Cu–Ni/$Al_2O_3$ catalysts (with 2.5 wt.% Ni).

tating anode X-ray generator (Ru-200B, Rigaku, Japan). A Ge(220) crystal was used as a monochromator with a 0.1 mm slit. Spectral resolution was about 5 eV at 9 keV incident energy. The thickness of the samples was adjusted so that the edge jump was $\simeq 1.5$. Pre-edge data were collected in steps of 5 eV for 100 eV and data up to 700 eV after the edge data were collected in steps of 1 eV (counting time at each point, 5 sec; total counts $> 10^5$). The EXAFS data were treated using the multiphasic model involving the additive relationship of the EXAFS function (*14*). EXAFS of the reference compounds, NiO, $NiAl_2O_4$, and CuO, were recorded under the same conditions after mixing them with appropriate quantities of $\gamma$-$Al_2O_3$ to achieve the same signal-to-noise ratio. The spectra of Ni and Cu metals were obtained from reduced NiO and CuO. In Table 1, we list the relevant data on the reference materials. Fourier transforms (FT) of the EXAFS data were carried out with $k_{min} \sim 3.5$ and $k_{max} \sim 11.0$ Å$^{-1}$ after weighting the data by $k^3$. In Fig. 2 we show typical raw EXAFS data for both Cu and Ni in the case of 2.5 wt.% Ni-variable Cu/$Al_2O_3$ reduced catalysts.

## RESULTS AND DISCUSSION

### *Ni K-edge*

We examine first the Ni EXAFS of the Ni/$\gamma$-$Al_2O_3$ catalyst since the results of this system are directly relevant to those obtained with the bimetallic Cu–Ni/$\gamma$-$Al_2O_3$ catalysts. Fourier transforms of the EXAFS data of Ni (5 wt.%)/$\gamma$-$Al_2O_3$ calcined at different temperatures showed that the first

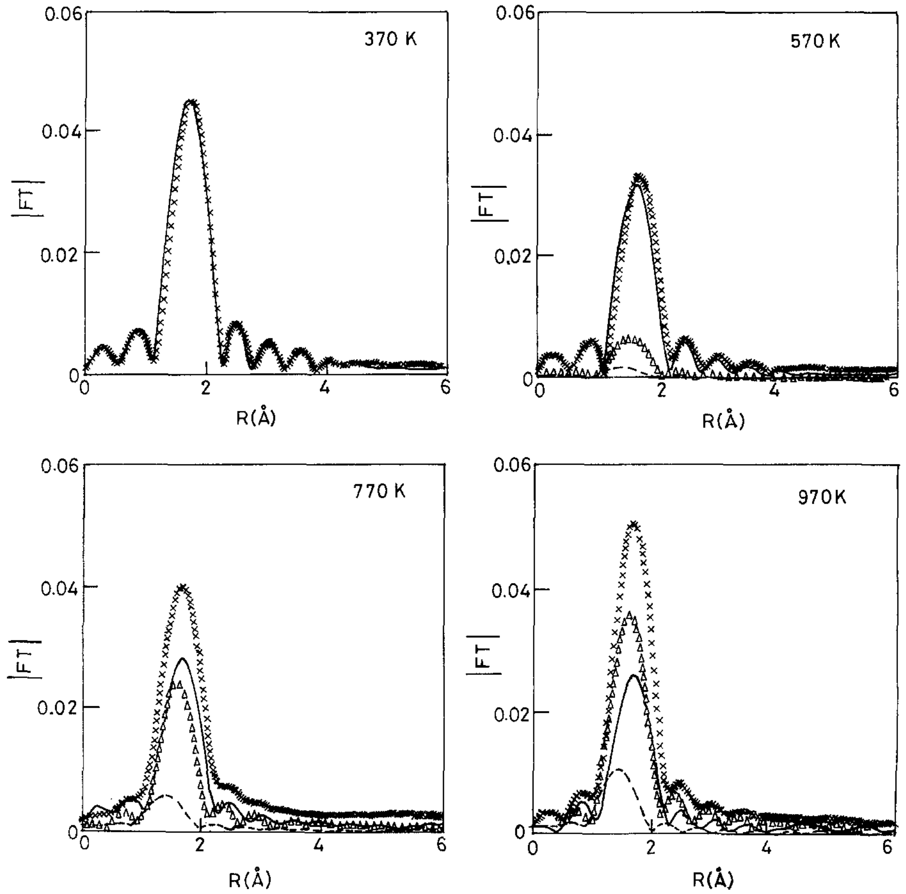

FIG. 3. Fourier deconvolution of the fitted Ni K-EXAFS data of Ni(5 wt.%)/γ-$Al_2O_3$ employing three Ni–O distances, calcined at different temperatures. Experimental, crosses; NiO-like phase, full line; Ni–O (tetrahedral) in $NiAl_2O_4$, broken line; Ni–O (octahedral) in $NiAl_2O_4$, triangles.

TABLE 2

Structural Parameters of Unreduced and Reduced Ni(5 wt.%)/γ-$Al_2O_3$[a]

| Calcination temperature (K) | Calcined systems | | | | | | | | | Reduced at 770 K | | | | | | | | |
|---|---|---|---|---|---|---|---|---|---|---|---|---|---|---|---|---|---|---|
| | Ni–O tet($NiAl_2O_4$) | | | Ni–O oct($NiAl_2O_4$) | | | Ni–O oct(NiO) | | | Ni–O(tet) | | | Ni–O(oct) | | | Ni–Ni(Ni metal) | | |
| | *N* | *R* | $\Delta\sigma^2$ | *N* | *R* | $\Delta\sigma^2$ | *N* | *R* | $\Delta\sigma^2$ | *N* | *R* | $\Delta\sigma^2$ | *N* | *R* | $\Delta\sigma^2$ | *N* | *R* | $\Delta\sigma^2$ |
| 370 | | | | | | | 6.0 | 2.11 | 0.001 | | | | 2.0 | 2.1[b] | 0.001 | 9.5 | 2.48 | 0.001 |
| 570 | 0.4 | 1.83 | 0.0 | 1.5 | 1.97 | 0.001 | 4.1 | 2.08 | 0.002 | 0.4 | 1.83[c] | 0.0 | 1.5 | 1.97[c] | 0.001 | 8.5 | 2.50 | 0.002 |
| 770 | 0.8 | 1.83 | 0.0 | 3.2 | 1.98 | 0.002 | 3.0 | 2.08 | 0.0 | 0.8 | 1.83[c] | 0.0 | 3.2 | 1.98[c] | 0.002 | 5.5 | 2.48 | 0.001 |
| 970 | 1.2 | 1.83 | 0.0 | 4.0 | 1.97 | 0.0 | 2.5 | 2.08 | 0.003 | 1.2 | 1.83[c] | 0.0 | 4.0 | 1.97[c] | 0.0 | 4.0 | 2.48 | 0.001 |

[a] The tet and oct stand for tetrahedrally and octahedrally coordinated Ni, respectively. *N*, *R*, and $\Delta\sigma^2$ stand for the coordination number, the interatomic distance, and the disorder term of the nearest neighbours.

[b] Pure NiO-like phase.

[c] $NiAl_2O_4$ phase.

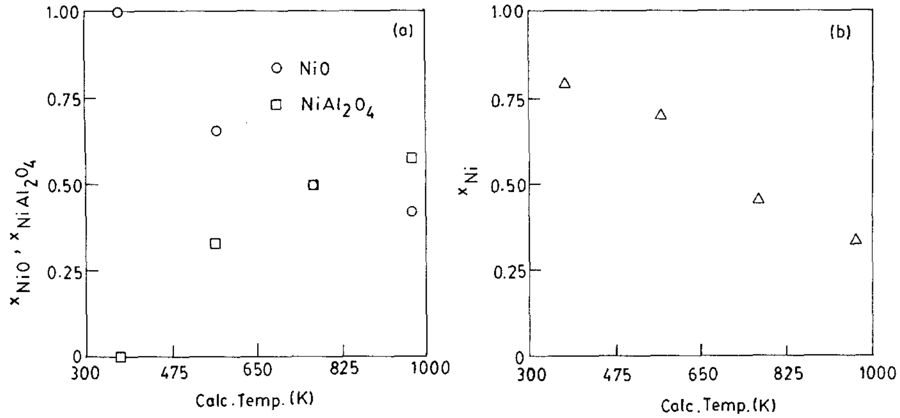

FIG. 4. (a) Variation of the fractions of NiO and $NiAl_2O_4$ in Ni (5 wt.%)/$\gamma$-$Al_2O_3$ with calcination temperature. (b) Variation of the fraction of metallic Ni produced on reduction with calcination temperature of Ni(5 wt.%)/$\gamma$-$Al_2O_3$.

peak in the Fourier transform shifts towards lower $r$-values with increasing calcination temperature. Accordingly, the sample dried at 370 K shows the first peak at 1.64 Å whereas that calcined at 970 K shows the peak maximum at 1.56 Å, indicating that Ni exists in a multiphasic environment in the calcined samples. Multiphasic curve-fitting analysis (*14*) was carried out on the inverse-transformed data ($r$-window, 1.2–2.0 Å) using the phase and amplitude parameters of Ni–O in NiO. The best fit was obtained when three Ni–O distances were used. Fourier deconvolution of the fitted data are shown in Fig. 3 and the results of the curve-fitting analysis are listed in Table 2. The sample dried at 370 K shows only the NiO-like octahedral environment for Ni. Peaks due to Ni with the tetrahedral and octahedral coordinations of $NiAl_2O_4$ develop progressively with increasing temperature of calcination (Table 2).

The compositions of the Ni/$\gamma$-$Al_2O_3$ samples calcined at different temperatures were calculated using the additive EXAFS relation,

$$\chi_{\text{total}}(k) = \sum_{i,m} x_i c_{i,m} \chi_{i,m}(k),$$

where $x_i$ is the fraction of the absorbing element in the $i$th phase ($\sum_i x_i = 1$) and $c_{i,m}$ is

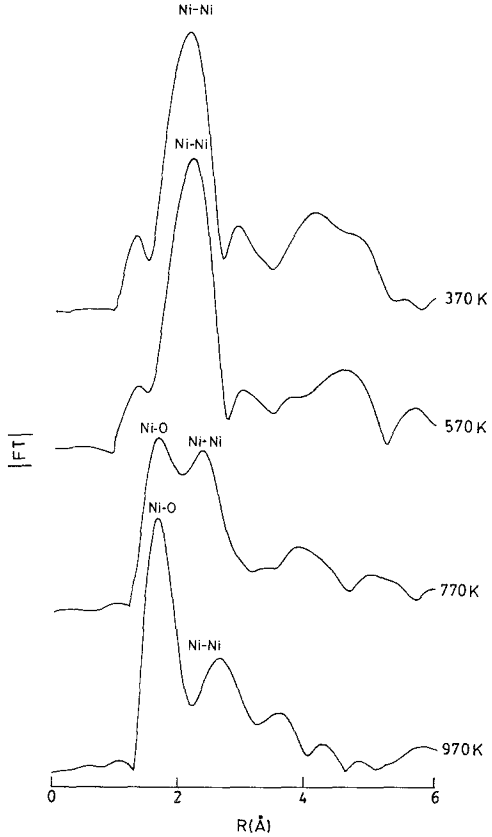

FIG. 5. Fourier transforms of Ni K-EXAFS of different samples of reduced Ni(5 wt.%)/$\gamma$-$Al_2O_3$ catalysts. Calcination temperatures of the different samples are shown.

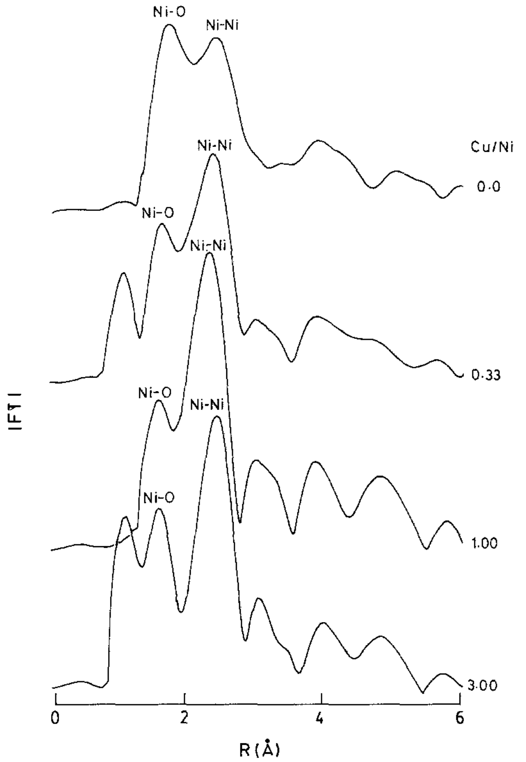

FIG. 6. Fourier transforms of Ni K-EXAFS of reduced Cu–Ni/$\gamma$-$Al_2O_3$ catalysts (with a total metal loading of 5 wt.%) with different Ni : Cu ratios.

the fraction of the absorbing element in the $m$th coordination of the $i$th phase ($\sum_m c_{i,m} = 1$). The above equation can be written in a more specific form as

$$\chi_{\text{total}}(k) = x_{\text{NiO}}\chi_{\text{NiO}}(k) + x_{\text{NiAl}_2\text{O}_4}(c_{\text{tet}}\chi_{\text{tet}}(k) + c_{\text{oct}}\chi_{\text{oct}}(k)).$$

Making use of the reference coordinations listed in Table 1 and the EXAFS results listed in Table 2, we have estimated the values of $x_{\text{NiO}}$, $x_{\text{NiAl}_2\text{O}_4}$, $c_{\text{tet}}$ and $c_{\text{oct}}$. The ratio of $c_{\text{tet}}$ to $c_{\text{oct}}$ has been found to be roughly 1 : 4, as expected of a mixed spinel. Interestingly $x_{\text{NiO}}$ decreases from 1.0 to 0.25 as the calcination temperature increases from 370 to 970 K accompanied by an increase in $x_{\text{NiAl}_2\text{O}_4}$ from 0.0 to 0.75. These results are shown in Fig. 4a to clearly demonstrate how the NiO content decreases with increase in the $NiAl_2O_4$ phase as the calcination temperature increases.

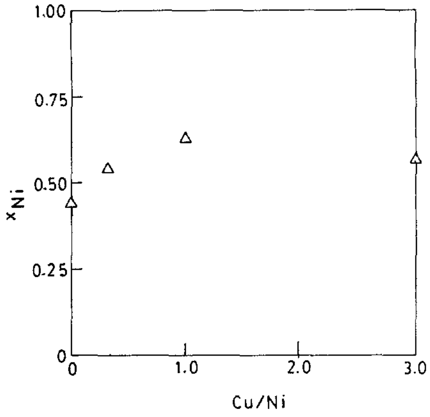

FIG. 7. Variation of the fraction of the Ni metal in the reduced Cu–Ni/$\gamma$-$Al_2O_3$ catalysts (with a total metal loading of 5 wt.%) with Cu/Ni ratio.

In Fig. 5 we show the Fourier transforms of the reduced samples of Ni/$\gamma$-$Al_2O_3$. Multiphasic analysis of the data was carried out with a $r$-window of 1.2–2.5 Å, employing the phase and amplitude parameters of Ni–O in NiO and Ni–Ni in Ni metal. The sample dried at 370 K becomes completely reduced to Ni (Table 2), whereas the sample calcined at 970 K shows little reduction. Employing the additive EXAFS relation,

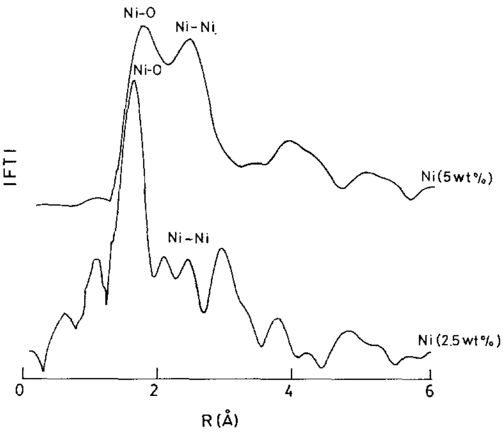

FIG. 8. Fourier transforms of Ni K-EXAFS of reduced Ni/$\gamma$-$Al_2O_3$ catalyst with different Ni loading.

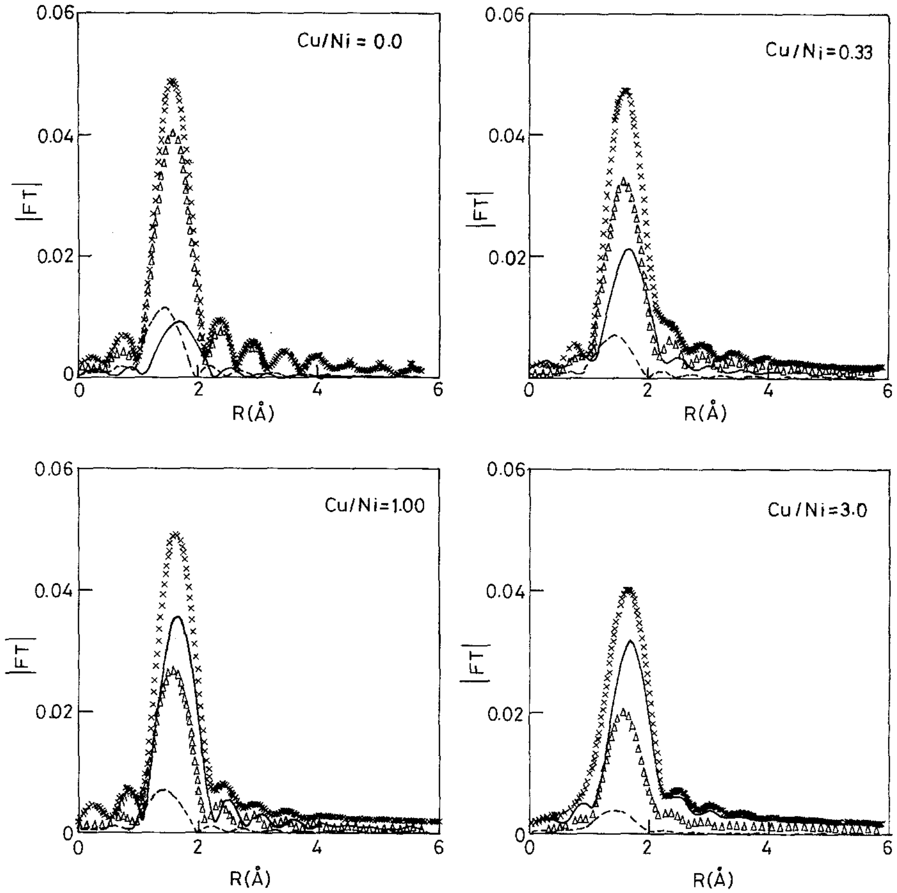

FIG. 9. Fourier deconvolution of the fitted Ni K-EXAFS data of Cu–Ni/$\gamma$-$Al_2O_3$ (fixed Ni loading of 2.5 wt.%) with different Cu loadings, employing three Ni–O distances. Symbols are same as in Fig. 2.

TABLE 3

Structural Parameters from Ni K-EXAFS of Unreduced and Reduced Cu–Ni/$\gamma$-$Al_2O_3$ Catalysts (with Fixed 2.5 wt.% Ni Loading)

| Catalyst with Ni : Cu | Calcined at 770 K | | | | | | | | | Reduced at 770 K | | | | | | | | |
|---|---|---|---|---|---|---|---|---|---|---|---|---|---|---|---|---|---|---|
| | Ni–O tet($NiAl_2O_4$) | | | Ni–O oct($NiAl_2O_4$) | | | Ni–O oct(NiO) | | | Ni–O tet($NiAl_2O_4$) | | | Ni–O oct($NiAl_2O_4$) | | | Ni–Ni (Ni metal) | | |
| | $N$ | $R$ | $\Delta\sigma^2$ | $N$ | $R$ | $\Delta\sigma^2$ | $N$ | $R$ | $\Delta\sigma^2$ | $N$ | $R$ | $\Delta\sigma^2$ | $N$ | $R$ | $\Delta\sigma^2$ | $N$ | $R$ | $\Delta\sigma^2$ |
| 100 : 0 | 1.0 | 1.84 | 0.0 | 4.0 | 1.97 | 0.0005 | 1.0 | 2.08 | 0.0005 | 1.0 | 1.84 | 0.0 | 4.0 | 1.97 | 0.001 | 2.7 | 2.5 | 0.0005 |
| 75 : 25 | 0.8 | 1.84 | 0.002 | 3.5 | 1.98 | 0.001 | 2.5 | 2.08 | 0.001 | 0.8 | 1.84 | 0.001 | 3.5 | 1.98 | 0.001 | 4.0 | 2.51 | 0.0003 |
| 50 : 50 | 0.8 | 1.84 | 0.0 | 2.5 | 1.97 | 0.001 | 3.2 | 2.08 | 0.0 | 0.8 | 1.84 | 0.0 | 2.5 | 1.97 | 0.001 | 7.5 | 2.54 | 0.0001 |
| 25 : 75 | 0.5 | 1.83 | 0.001 | 2.0 | 1.97 | 0.002 | 3.5 | 2.08 | 0.004 | 0.5 | 1.83 | 0.0 | 2.0 | 1.97 | 0.002 | 9.0 | 2.53 | 0.001 |

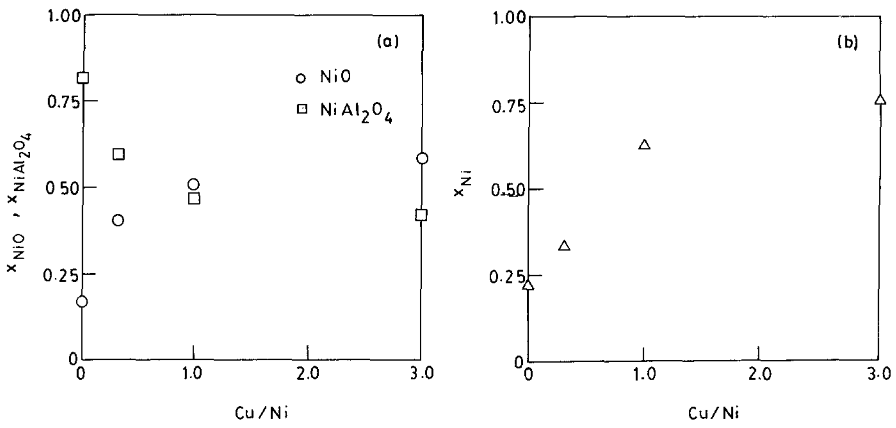

FIG. 10. (a) Variation of the fractions of NiO and $NiAl_2O_4$ of calcined Cu–Ni/$\gamma$-$Al_2O_3$ catalysts (fixed Ni loading of 2.5 wt.%) with Cu/Ni ratio. (b) Variation of the fraction of metallic Ni produced on reduction of Cu–Ni/$\gamma$-$Al_2O_3$ (fixed Ni loading of 2.5 wt.%) with Cu/Ni ratio.

$$\chi_{\text{total}}(k) = x_{\text{Ni}}\chi_{\text{Ni}}(k) + x_{\text{NiO}}\chi_{\text{NiO}}(k) + x_{\text{NiAl}_2\text{O}_4}(c_{\text{tet}}\chi_{\text{tet}}(k) + c_{\text{oct}}\chi_{\text{oct}}(k)),$$

we have obtained $x_{\text{Ni}}$ in the reduced samples. The results are presented in Fig. 4b. Assuming no reduction in Ni–Ni coordination of the reduced phase due to particle size effects, we find the amount of Ni metal in the reduced sample to be roughly proportional to that of the NiO-like phase in the calcined sample; $NiAl_2O_4$ is obviously not reduced readily at 770 K. We conclude that the reducibility of Ni in the Ni/$\gamma$-$Al_2O_3$ catalyst depends on the concentration of the NiO-like phase in the calcined sample.

We now examine the promotion effect of Cu towards the reduction of nickel in the bimetallic Cu–Ni/$\gamma$-$Al_2O_3$ catalysts. While studying bimetallic catalysts as a function of the relative concentration of the metals, it is customary to keep the total metal loading constant, and vary the ratio of the two metals. Type 2 catalysts (see Experimental section) discussed in this paper belong to this category. Fourier transforms of the Ni K-EXAFS of the Type 2 Cu–Ni/$\gamma$-$Al_2O_3$ catalysts with a total metal loading of 5 wt.%, reduced at 770 K for 3 h are shown in Fig. 6. We see that catalysts containing Cu undergo greater reduction of Ni than the pure Ni/$\gamma$-$Al_2O_3$ catalyst. The extent of re-

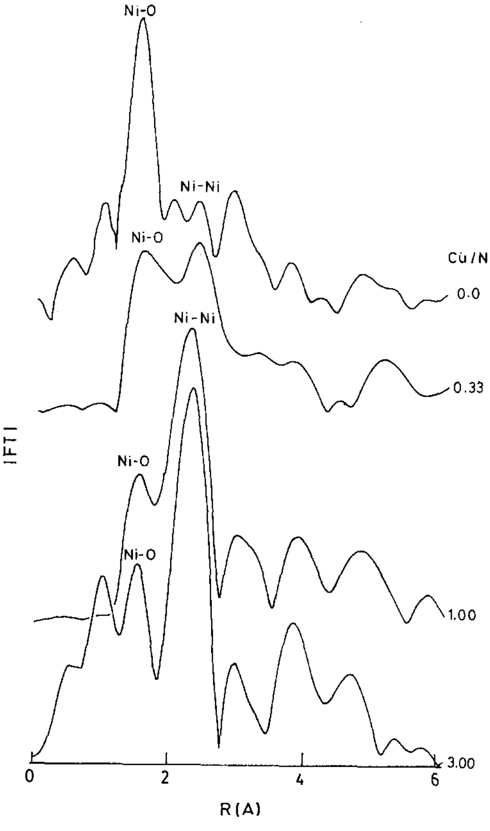

FIG. 11. Fourier transforms of Ni K-EXAFS of reduced Cu–Ni/$\gamma$-$Al_2O_3$ catalysts (fixed Ni loading of 2.5 wt.%) with different Cu loadings.

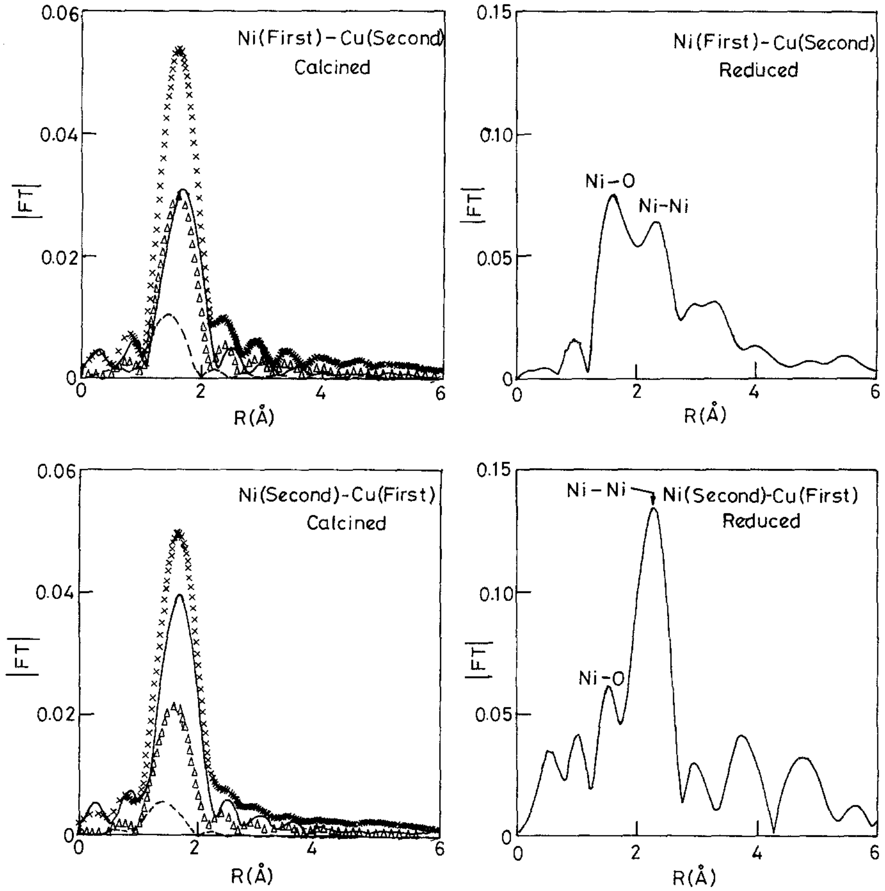

FIG. 12. Fourier deconvolution of the fitted Ni K-EXAFS data of two-stage impregnated Cu–Ni/$\gamma$-$Al_2O_3$ (Cu/Ni = 0.5, each 2.5 wt.%). Fourier transforms of Ni K-EXAFS of these catalysts on reduction are also shown.

duction of Ni was estimated by multiphasic curve-fitting analysis and the results are presented in Fig. 7 as a function of the relative proportion of Cu in the catalyst. The catalyst with a Ni : Cu ratio of 50 : 50 seems to show the maximum reduction. This observation can be understood if one takes into account the variation in the reducibility of Ni/$\gamma$-$Al_2O_3$ with Ni–metal loading. In Fig. 8 we show the Fourier transforms of reduced Ni/$\gamma$-$Al_2O_3$ with 2.5 wt.% and 5 wt.% loading. One readily sees that the catalyst with 5 wt.% metal loading undergoes greater reduction.

In order to understand more fully the reducibility of Ni with Cu loading, we have studied Cu-Ni/$\gamma$-$Al_2O_3$ catalysts with a fixed Ni loading of 2.5 wt.%, but with varying Ni/Cu ratios (Type 3 preparation, see Experimental section). Multiphasic curve-fitting analysis employing three Ni–O distances was carried out on the inverse Fourier-transformed data; Fourier deconvolutions of the fitted data are shown in Fig. 9. We find that with increasing Cu loading, the proportion of the NiO-like phase increases and is accompanied by a decrease in the $NiAl_2O_4$-like phase (see Table 3 and Fig. 10a). The Fourier transforms of these catalysts after reduction show that the extent of reduction to metallic Ni increases from ~25% (in the absence of any Cu in Ni/

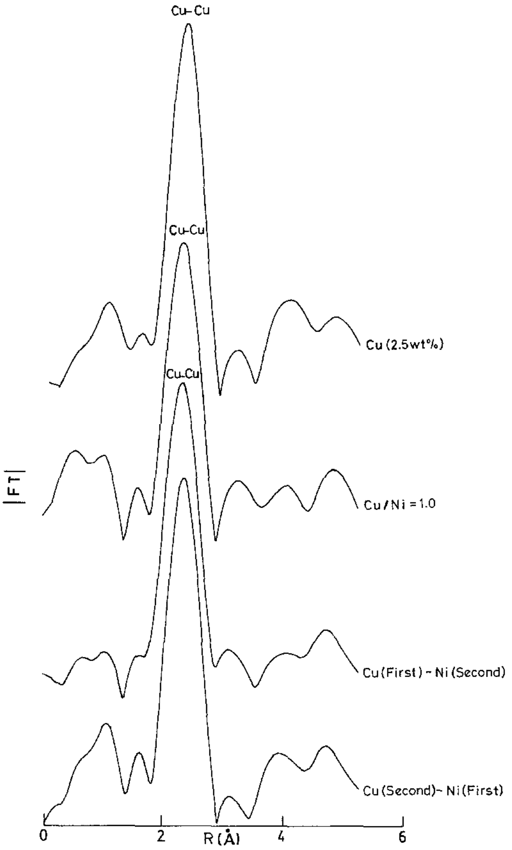

FIG. 13. Fourier transforms of Cu K-EXAFS of some Cu catalysts after reduction.

$Al_2O_3$) to nearly 75% when the Cu/Ni ratio is 75/25 (Fig. 11). In Fig. 10b we depict the variation of metallic Ni obtained on reduction with Cu/Ni ratio. This is also reflected in the decrease in the white-line intensity with increasing Cu content in the raw EXAFS data (Fig. 2).

Comparing Figs. 10(a) and (b), we see that the proportion of reduced Ni formed is directly proportional to the NiO-like phase present before reduction. This would imply that if one can, by some means, prevent the $Ni^{2+}$ ions from interacting with $\gamma$-$Al_2O_3$ during calcination, thereby preferentially promoting the formation of the NiO-like phase (instead of the $NiAl_2O_4$-like phase), there would be greater proportion of metallic Ni on reduction. We would confirm this conjecture by two-stage impregnations of the bimetallic catalysts (Type 4, see Experimental section). In Fig. 12 we show the Fourier transforms of the Ni K-EXAFS of the two-stage impregnated samples before and after reduction. The coordination number of Ni in the NiO-like phase is low (2.7) after calcination in the sample where Ni was first impregnated compared to that (3.6) where Cu was first impregnated. The Fourier transforms of the reduced catalysts show that the reduction to metallic Ni is significantly higher in the case where Cu was first impregnated. Accordingly, the Ni–Ni coordination is 8.3 in this case compared to that when Ni was first impregnated (4.0). These observations establish that the promotion effect of Cu on Ni is through enhancing the formation of the NiO-like phase during calcination.

### *Cu K-EXAFS*

Copper in all copper-containing systems undergoes almost complete reduction, as also indicated by the absence of the white-line in the EXAFS (Fig. 2). In Fig. 13 the Fourier transforms of some of the copper systems after reduction are illustrated. The Cu–Cu distance in the reduced samples does not differ much from that of the Cu metal bulk; there is about 25% reduction in the Cu–Cu coordination which accounts for the dispersion of metallic Cu on $\gamma$-$Al_2O_3$.

## CONCLUSIONS

From our study of Ni/$\gamma$-$Al_2O_3$ calcined at different temperatures, we find that Ni interacts with $\gamma$-$Al_2O_3$ during calcination, Ni being present mainly in the highly dispersed NiO-like phase at low calcination temperatures. With an increase in the calcination temperature, Ni ions form $NiAl_2O_4$ by interaction with the support. The higher the calcination temperature, the greater is the proportion of the aluminate phase. The metallic Ni formed after reduction is almost entirely due to the reduction of the NiO-like phase (Fig. 4a and b). The NiO phase in the calcined samples and the Ni metal in the reduced samples vary similarly with the calcination temperature.

At low metal loadings, Ni tends to form the aluminate (*11*). When surface saturation is reached, NiO segregates out. The percentage reduction of Ni, therefore, increases with the metal loading. Coimpregnating with Cu results in partially covering the $\gamma$-$Al_2O_3$ surface with a CuO-like or $CuAl_2O_4$-like phase, thereby decreasing the formation of the $NiAl_2O_4$ phase. We, therefore, see that with increasing Cu-content (at fixed Ni loading), the proportion of the NiO-like phase in the calcined state as well as the formation of metallic Ni on reduction increase. It is to be noted that Cu in the form of dispersed CuO or $CuAl_2O_4$ is more easily reducible than the surface Ni aluminate. The idea that in bimetallic Cu–Ni catalysts Cu acts as a barrier for Ni to interact with $\gamma$-$Al_2O_3$, is further confirmed by two-stage impregnation experiments. When the support is first impregnated with Cu, it covers the $\gamma$-$Al_2O_3$ surface and Ni subsequently introduced remains in the dispersed NiO-like phase which then becomes reduced readily to Ni metal.

## ACKNOWLEDGMENTS

The authors thank the Department of Science and Technology and the University Grants Commission for support of this research. One of the authors (GUK) thanks the Council for Scientific and Industrial Research for a research fellowship.

## REFERENCES

1. Charcosset, H., Frety, R., Soldat, A., and Trambouze, Y., *J. Catal.* **22,** 204 (1971).
2. Roman, A., and Delmon, B., *J. Catal.* **30,** 333 (1973).
3. (a) Gentry, S. J., Hurst, N. W., and Jones, A., *J. Chem. Soc. Faraday Trans. 1* **77,** 603 (1981); (b) Sinfelt, J. H., Via, G. H., Lytle, F. W., *Catal. Rev. Sci. Eng.* **26,** 81 (1984).
4. Gharpurey, M. K., and Emmett, P. H., *J. Phys. Chem.* **65,** 1182 (1961).
5. Sachtler, W. M. H., and van der Plank, P., *Surf. Sci.* **18,** 62 (1969).
6. Carr, P. F., and Clarke, J. K. A., *J. Chem. Soc. A* **985** (1971)
7. Bartholomew, C. H., Pannell, R. B., and Fowler, R. W., *J. Catal.* **79,** 34 (1983).
8. Lo Jacono, M., Schiavello, M., and Cimino, A., *J. Phys. Chem.* **75,** 1044 (1971).
9. (a) Greegor, R. B., Lytle, F. W., Chin, R. L., and Hercules, D. M., *J. Phys. Chem.* **85,** 1232 (1981); (b) Friedman, R. M., Freeman, J., Lytle, F. W., *J. Catal.* **55,** 10 (1978).
10. Ertl, G., Hierl, R., Knözinger, H., Thiel, N., and Urbach, H. P., *Appl. Surf. Sci.* **5,** 49 (1980).
11. de Bokx, P. K., Wassenberg, W. B. A., and Geus, J. N., *J. Catal.* **104,** 86 (1987).
12. Bernardo, C. A., Alstrup, I., and Rostrup-Nielsen, J. R., *J. Catal.* **96,** 517 (1985).
13. Sankar, G., Vasudevan, S., and Rao, C. N. R., *J. Phys. Chem.* **90,** 5325 (1986).
14. (a) Kulkarni, G. U., Sankar, G., and Rao, C. N. R., *Z. Phys. B.: Condens. Matter* **73,** 529 (1989); (b) Sankar, G., Kulkarni, G. U., and Rao, C. N. R., *Prog. Cryst. Growth Charact.* **18,** 67(1989).